Terrestrial Free Space Optical Communication Systems Availability based on Meteorological Visibility Data for South Africa

Olabamidele O. Kolawole, *Student Member, IEEE*, Thomas J. O. Afullo, *Senior Member, IEEE*, and Modisa Mosalaosi, *Member, IEEE*

***Abstract*—In spite of the numerous advantages of employing free space optical (FSO) communication systems as viable complementary platforms for next-generation networks, the presence of atmospheric disturbances such as fog and scintillations are major sources of signal impairment which degrade system performance. Consequently, it becomes imperative to investigate and contextualize the unique climatic conditions in those locations where FSO links are to be deployed. Statistical evaluation of meteorological visibility data collected for various cities in South Africa is thus hereby employed in estimating the availability performance of FSO links transmitting at both 850 nm and 1550 nm. It is determined that the cities of Mbombela and Cape Town have the lowest performance due to the high occurrence of fog events as compared to other regions in South Africa. During foggy periods, FSO links in Mbombela and Cape Town would have availabilities of ~99.6% for link distances of 500 and 600 metres, respectively. The bit error rate (BER) estimations of intensity modulation and direct detection (IM/DD) FSO links in the presence of weak atmospheric turbulence were also investigated for the identified locations during foggy weather; with the cities of Mafikeng and Kimberley showing the lowest BER performances because of their high wind velocities, altitudes and refractive index values. In order to obtain a BER of 10^{-6}, receive signal-to-noise ratio (SNR) values ranging from ~46 to ~51 dB are required for FSO links deployed for data transmission in the various cities investigated in this work.**

***Index Terms*—Aerosol scattering attenuation, atmospheric turbulence, BER, FSO, link availability, minimum required visibility.**

I. INTRODUCTION

RISING urbanization, population growth, increase in housing costs, and demand for higher standards of living have generated an urgent need for smart cities to maximize resource use [1]. Based on the International Mobile Telecommunications 2020 (IMT-2020) vision of the International Telecommunication Union (ITU), the fifth generation (5G) technology is expected to support enhanced mobile broadband (eMBB) with throughputs up to 10 Gbits/s, massive machine type communication (mMTC) for up to 1 million connections per square km, and ultra-reliable low latency communication (uRLLC) as low as 1 ms. This is to ensure that intelligent traffic systems, internet of vehicles (IoV), and internet of things (IoT) connections in emerging smart cities function optimally. 5G technology is also needed to meet the high requirements on speed for virtual reality (VR), augmented reality (AR) and mixed reality (MR) applications [2]-[4].

FSO communication is a viable complementary solution platform for next-generation communication networks, whether as a standalone or hybrid technology. When employed in 5G cellular backhaul networks, its numerous advantages include: flexible network connectivity, secure transmission, high data throughput, ease of installation, relative low cost of deployment, immunity to electromagnetic interference, license-free spectrum, low latency communication, low bit error rate (BER), etc. [5]. Despite these numerous merits, the performance of FSO links is severely affected by weather constraints. Aerosol scattering attenuation due to fog and atmospheric turbulence due by scintillations are major sources of signal impairment, hence impacting on the received signal quality [1], [5], [6].

Hybrid FSO - Millimeter wave (FSO/MMW) links for FSO-based backhaul networks have been proposed in literature. These are aimed at obtaining reliable and uninterrupted network connectivity by switching between the main FSO link and the backup MMW link whenever the main FSO link is unavailable due to weather constraints. Dual FSO thresholds are incorporated in the system to prevent unnecessary switching between links [6].

This paper was submitted for review on the 7th of June, 2021.

O. O. Kolawole is with the School of Electrical, Electronics and Computer Engineering, Howard College Campus, University of KwaZulu-Natal, Durban, South Africa (e-mail: kolawole.olabamidele@gmail.com).

T. J. O. Afullo is with the School of Electrical, Electronics and Computer Engineering, Howard College Campus, University of KwaZulu-Natal, Durban, South Africa (e-mail: afullot@ukzn.ac.za)

M. Mosalaosi is with the Department of Electrical, Computer and Telecommunication Engineering, Botswana International University of Science and Technology, Palapye, Botswana (e-mail: mosalaosim@biust.ac.bw).

Creative Commons License: CC BY

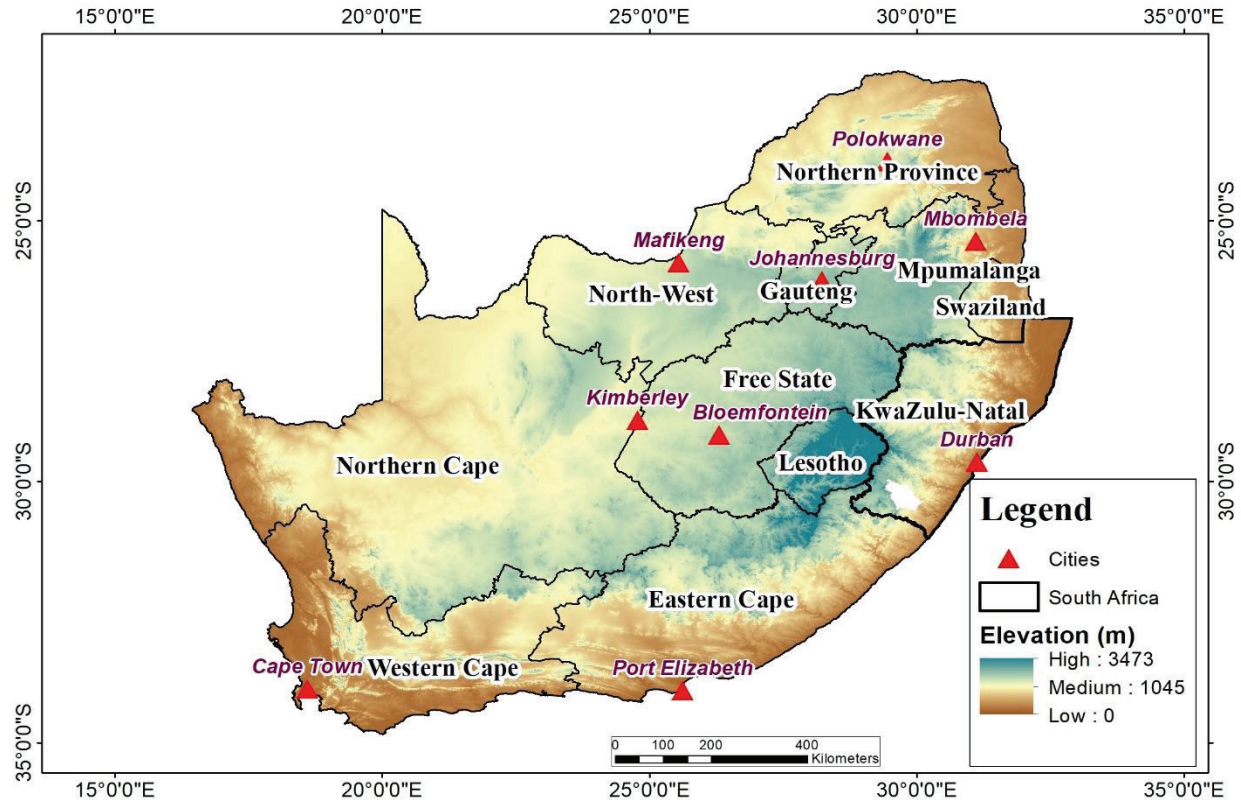

Fig. 1. Map of South Africa showing elevation above sea level and locations of selected cities investigated in this work.

In [7], the performance analysis of a FSO/MMW system incorporated with a flying network platform (FNP) which employs point to point FSO/MMW links to pass backhaul traffic between the access and core networks is carried out. While the results obtained in [6]-[7] indicate that the proposed hybrid FSO links outperform the single FSO link, it is important to state that thorough estimations of signal losses based on the climatic constraints of the various locations where the links are to be deployed was not done. This is imperative in determining the switching thresholds of the proposed links which may differ from one location to another.

South Africa's climate is considered highly variable spatially and temporally. The spatial differences in elevation across the country play an important part in this variability (Fig. 1). Locations of the various cities investigated in this work are highlighted in Fig. 1 across the South African geographical space. According to the Köppen-Geiger climate classification for South Africa developed by the Council for Scientific and Industrial Research (CSIR), the country is classified predominantly as semi-arid, with influences from temperate and tropical zones [8]-[9]. Mafikeng, Kimberley and Bloemfontein have northern steppe climates; Bloemfontein has cold arid weather while Mafikeng and Kimberley are majorly arid and hot. Johannesburg and Mbombela have mild temperate climates with the former being high-veld while the latter is low-veld. Durban has a humid subtropical climate while Cape Town is classified as a Mediterranean climate with warm summers and wet winters. Polokwane has a Bush-veld climate that is arid, with hot summers and cold winters while Port Elizabeth has a southern coastal climate characterized by rain during all seasons [10]-[12].

TABLE I
DESCRIPTION OF THE CLIMATE OF SELECTED CITIES IN SOUTH AFRICA [8]-[12].

City	Climate
Bloemfontein	Northern Steppe (Arid and cold)
Cape Town	Mediterranean
Durban	Subtropical
Johannesburg	High-veld (Warm Temperate)
Kimberley	Northern Steppe (Arid and Hot)
Mafikeng	Northern Steppe (Arid and Hot)
Mbombela	Low-veld (Temperate)
Polokwane	Bush-veld (Arid and Hot)
Port Elizabeth	Southern Coastal Belt

Most of the proposed FSO and hybrid FSO systems in literature are constrained in their ability to estimate the losses encountered by FSO links in every location they are to be deployed. The focus of this paper is in determining the attenuations based on the atmospheric conditions prevalent in all the climatic zones of South Africa. It is also important to state that the cities chosen are urban places with considerable population, hence great demand for high data rates and fast internet connectivity.

The following are the key contributions of this work:

1) Cumulative distribution of visibility and aerosol scattering attenuations based on the Ijaz and Kim models for transmission wavelengths of 850 and 1550 nm in nine cities of South Africa are presented.
2) Probabilities of exceedance, deceedance and encountering

of different aerosol scattering attenuations for 850 and 1550 nm are calculated and their impact on FSO link performance investigated for all the various locations of interest.

3) Modeling of the minimum required visibility CDFs during foggy and clear weather conditions are presented. To the best of our knowledge, approximate polynomial expressions for determining the minimum required visibilities for FSO systems transmitting at 1550 nm in various locations have not been reported in open literature so far.
4) Determined link availability performances for two commercial FSO links are presented during foggy and clear weather conditions.
5) Numerical expressions for obtaining the BER for FSO systems employing IM/DD with non-return-to-zero on-off keying (NRZ-OOK) modulation under the influence of weak turbulence are presented. Achievable SNRs and data rates of the two FSO links are also investigated.

The rest of this paper is structured as follows: Section II presents the visibility distribution of nine cities in South Africa; Section III presents and analyzes the cumulative distribution of aerosol scattering attenuation based on the Kim and Ijaz models for the two transmission wavelengths in the locations of interest, with the probabilities of exceedance, deceedance and encountering of various scattering attenuations calculated and discussed therein. The link budgets for two commercial FSO communication systems are provided in Section IV; while Section V presents the minimum required visibility CDFs with the corresponding polynomial coefficients. The approximate expressions for evaluating the link availability performance are determined in Section VI. In Section VII, the SNR, BER and data rate equations of received signals for FSO links in a weak turbulence regime are derived and their results analyzed; while the conclusions are presented in Section VIII.

II. Visibility Distribution

The scattering and absorption of optical signals is strongly impacted by visibility. Meteorological visibility may be defined as the distance in the atmosphere at which a fraction of the luminous flux transmitted by a collimated beam emanating from a 550 nm light source is reduced to 5% of its value. In other words, it is the optical range determining how far away objects can be seen under certain weather conditions such as snow, rain, haze etc.[13]-[14]. The presence of suspended fine water droplets in the atmospheric layer closest to the surface of the earth results in the formation of fog. Fog is a weather condition where visibility drops below 1000 m and the atmospheric humidity approaches 100% [15].

Visibility data from January 2010 till June 2018 was obtained for major cities in each of the nine provinces of South Africa from the South Africa Weather Service (SAWS). These urban areas of interest are Bloemfontein, Cape Town, Durban, Johannesburg, Kimberley, Mafikeng, Mbombela, Polokwane and Port Elizabeth. The data was collected three times daily

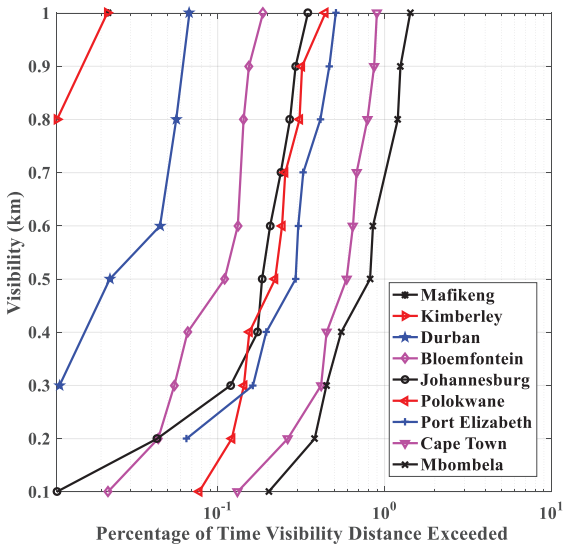

(a) Visibility under fog conditions

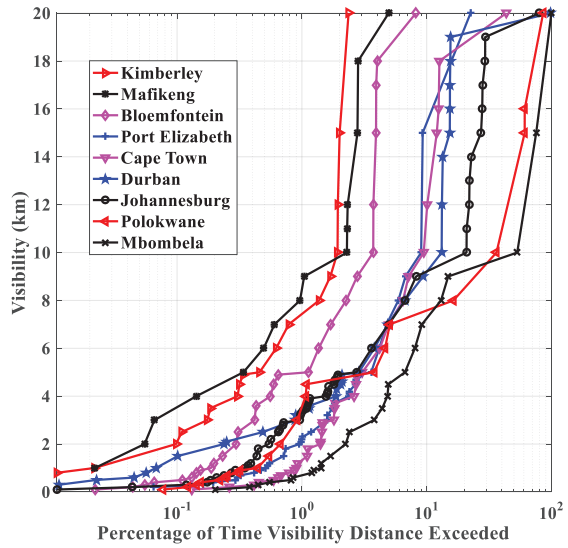

(b) Visibility up to 20 km

Fig. 2. Visibility against percentage of time visibility distance exceeded for various cities in South Africa from January 1, 2010 to June 30, 2018 under (a) fog conditions and (b) haze and clear weather conditions.

(8:00 a.m., 2:00 p.m. and 8:00 p.m.) for the 8½ year period.

Fig. 2(a) shows the visibility under fog conditions (0 to 1 km) against the percentage of time the visibility events took place while Fig. 2(b) shows the duration of visibility events up to 20 km over the time period investigated for all the selected locations in South Africa. In Fig. 2(a), Mbombela and Cape Town have fog events that last up to 1% of the time considered, while Port Elizabeth, Polokwane, Johannesburg, and Bloemfontein experience foggy events less than 0.5% of the time. Foggy incidents occur less than 0.07% of the time for Durban, Kimberley, and Mafikeng, according to the processed data. Fig. 2(b) best captures the visibility under haze and clear weather conditions. The cities of Mbombela, Cape Town, Port

Elizabeth, Polokwane and Johannesburg all have more visibility events under haze conditions than Kimberley, Mafikeng and Durban. Cumulative distributions of visibility based on average worst month, year and hour measurements for the same cities are shown in [16].

III. Scattering Attenuation

The Beer-Lamberts law can be used to model the propagation of optical signals across the atmosphere. It is stated in [17] as:

$$\tau(\lambda, L) = e^{-(\alpha L)} \tag{1}$$

where $\tau(\lambda, L)$ is the transmittance of the atmosphere in (km^{-1}), α represents the atmospheric attenuation coefficient or total extinction coefficient, λ is the wavelength of the optical signal in nm and L is the distance of propagation in km. The Kruse model is used to calculate the coefficient of atmospheric attenuation from visible to near-infrared wavelengths. It is expressed as [17]-[18]:

$$\alpha = \frac{-\ln(T_{th})}{V}\left(\frac{\lambda}{\lambda_\circ}\right)^{-q_\circ} = \frac{3.912}{V}\left(\frac{\lambda}{\lambda_\circ}\right)^{-q_\circ} \tag{2}$$

where $T_{th} = 2\%$ is the optical threshold, $\lambda_\circ = 550nm$ is the solar band's maximum spectrum wavelength, λ is the wavelength of the optical signal in nm, V is the meteorological visual range in km and $q_\circ$ represents the particle size distribution parameter. The total extinction coefficient in decibel per unit length is given as:

$$\alpha_a(V) = \alpha 10\log_{10}(e) \approx 4.343\alpha \tag{3}$$

As optical signals traverse the free space media, discontinuities in the atmosphere, such as aerosols and gas molecules, act as sources of reduced signal power. Scattering losses, also known as atmospheric attenuation, are caused by these channel impediments and are calculated using [19]:

$$A_a(L,V) = \alpha_a(V) \times L \tag{4}$$

Since the aerosol scattering coefficient is the most influential atmospheric channel parameter for scattering losses in optical signals, the atmospheric attenuation is approximately equal to the aerosol scattering coefficient [19]-[20], that is:

$$\alpha_a(V) \cong \beta_{sa}(\lambda) \tag{5}$$

The aerosol scattering coefficient or specific atmospheric attenuation in dB/km, as given in [16]-[17] is:

$$\beta_{sa}(\lambda) = 10\log_{10}(e)\left(\frac{3.912}{V}\right)\left(\frac{\lambda}{\lambda_\circ}\right)^{-q_\circ} = \frac{17}{V}\left(\frac{\lambda}{\lambda_\circ}\right)^{-q_\circ} \tag{6}$$

Equation (6) describes the Kim and Ijaz fog models. In the Kim model, the particle size distribution parameter, $q_\circ$, is expressed in terms of all forms of visibility as [21]:

$$q_\circ(V) = \begin{cases} 1.6 & for \quad V > 50km \\ 1.3 & for \quad 6 < V < 50km \\ 0.16V + 0.34 & for \quad 1 < V < 6km \\ V - 0.5 & for \quad 0.5 < V < 1km \\ 0 & for \quad V < 0.5km \end{cases} \tag{7}$$

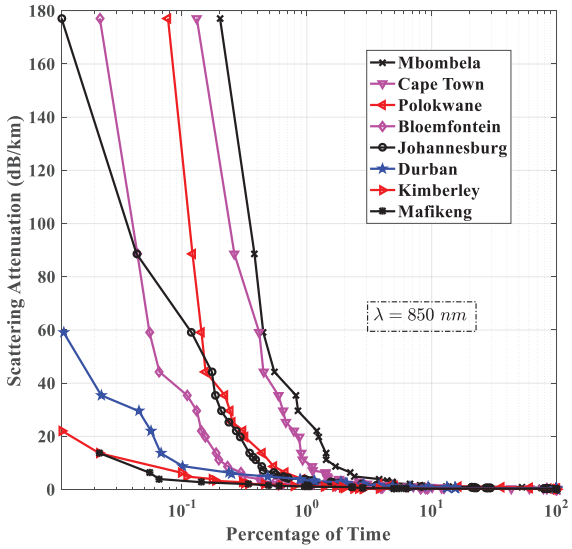

(a) 850 nm

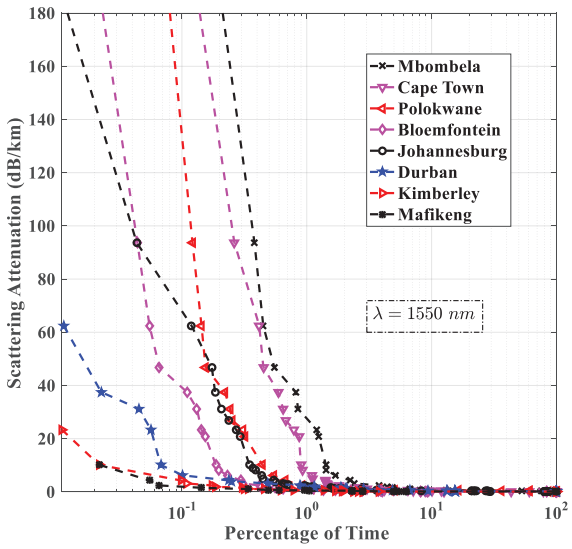

(b) 1550 nm

Fig. 3. Cumulative distribution of Aerosol scattering attenuation for major cities in South Africa using Ijaz's and Kim's models from January 1, 2010 to June 30, 2018 for (a) 850 nm and (b) 1550 nm.

For the Ijaz fog model, on the other hand, $q_\circ$, is given in terms of wavelength as [22]-[23]:

$$q_\circ(\lambda) = 0.1428\lambda - 0.0947 \tag{8}$$

Figs. 3(a) and (b) show the cumulative distributions of scattering attenuation for major cities in South Africa. For visibility measurements less than 1 km, the Ijaz model was used to calculate scattering losses, while the Kim model was used to calculate the specific attenuation associated with visibility values greater than or equal to 1 km. The two models were used to estimate scattering losses encountered by transmission wavelengths of 850 and 1550 nm. In both figures, the cities of Johannesburg, Bloemfontein, Polokwane, Cape Town and

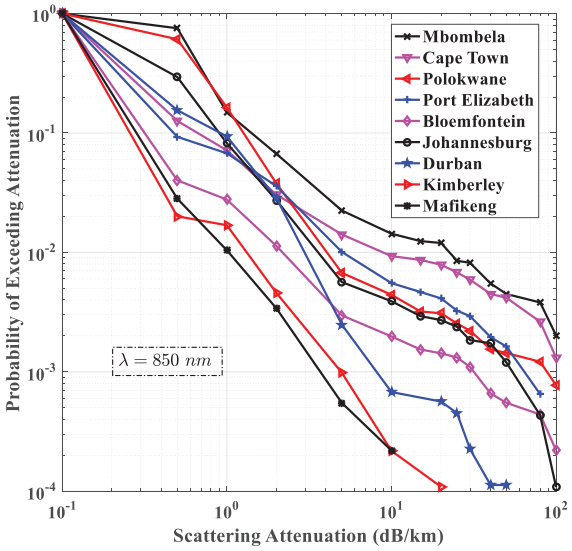

(a) 850 nm

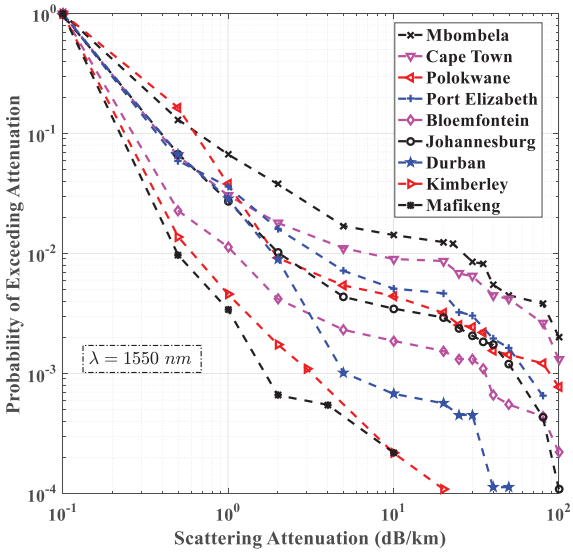

(b) 1550 nm

Fig. 4. Probability of exceeding different atmospheric scattering attenuation conditions for major cities in South Africa for (a) 850 nm and (b) 1550 nm.

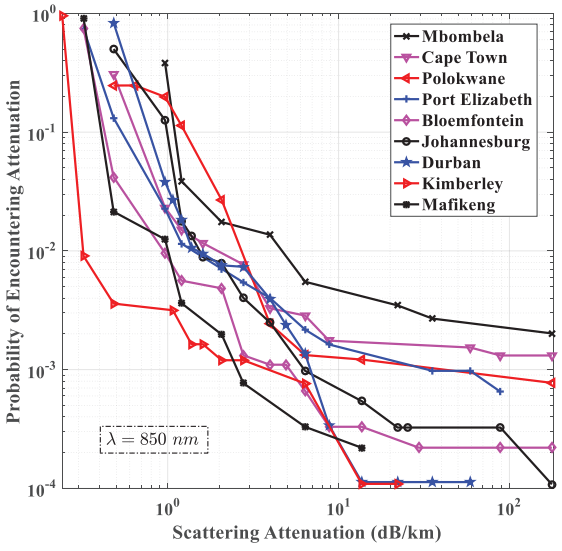

(a) 850 nm

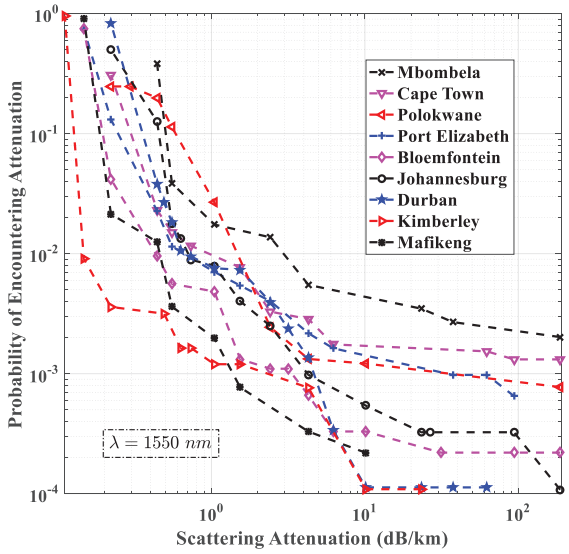

(b) 1550 nm

Fig. 5. Probability of encountering different atmospheric scattering attenuation conditions for major cities in South Africa for (a) 850 nm and (b) 1550 nm.

Mbombela encounter scattering attenuation greater than 175 dB/km for periods ranging from 0.01 % to 0.2 % of the entire time considered. Specific attenuation below 100 dB/km was observed in Durban, Kimberley, and Mafikeng for periods less than 0.07 % of the time investigated.

Before deploying an FSO system, it is critical to understand the weather constraints that will be faced in a given area and at a given time. Once the maximum attenuation the FSO system can tolerate is determined, the FSO system installer can predict the likelihood of system outage based on the probability of exceeding and encountering a specific atmospheric attenuation value. The probabilities of exceeding different scattering attenuation losses for 850 nm and 1550 nm wavelength systems are shown in Figs. 4(a) and (b). In the cities of Mbombela, Cape Town and Polokwane, FSO systems transmitting at the two wavelengths have a likelihood of facing attenuation values greater than 80 dB/km with probabilities of 0.0038, 0.0026 and 0.0012, respectively.

The probabilities of FSO links encountering different atmospheric attenuations when transmitting at 850 nm and 1550 nm are shown in Figs. 5(a) and (b). The probability of FSO links encountering scattering losses of 177 dB/km and 187 dB/km at these wavelengths in Mbombela, Cape Town,

TABLE II
Most frequent fog measurements and their associated probabilities for major cities in South Africa.

Location	Most Frequent Fog Events (km)	Attenuation (dB/km) - 850 nm	Attenuation (dB/km) – 1550 nm	Probability of Encountering Scattering Attenuation (-)	Probability of Exceedance (-)
Cape Town	0.3	59.05	62.51	0.001534	0.004163
Port Elizabeth	0.5	35.43	37.51	0.000976	0.002929
Durban	0.6	29.53	31.25	0.000226	0.000451
Bloemfontein	0.5	35.43	37.51	0.000440	0.001100
Kimberley	0.8	22.14	23.44	0.000109	0.000109
Johannesburg	0.3	59.05	62.51	0.000759	0.001193
Mafikeng	1	13.67	10.13	0.000219	0.000219
Mbombela	0.8	22.14	23.44	0.003475	0.011993
Polokwane	0.5	35.43	37.51	0.000663	0.002209

TABLE III
Most frequent visibility measurements and their associated probabilities for major cities in South Africa.

Location	Most Frequent Visibility (km)	Attenuation (dB/km) - 850 nm	Attenuation (dB/km) - 1550 nm	Probability of Encountering Scattering Attenuation (-)	Probability of Deceedance (-)
Cape Town	20	0.4827	0.2210	0.3075	0.8737
Port Elizabeth	30	0.3218	0.1474	0.7421	0.7437
Durban	20	0.4827	0.2210	0.8323	0.8448
Bloemfontein	30	0.3218	0.1474	0.7453	0.9079
Kimberley	40	0.2413	0.1105	0.9618	0.9623
Johannesburg	20	0.4827	0.2210	0.5010	0.7060
Mafikeng	30	0.3218	0.1474	0.9135	0.9379
Mbombela	10	0.9653	0.4421	0.3822	0.8514
Polokwane	15	0.6436	0.2947	0.2475	0.6381

Polokwane, Bloemfontein, and Johannesburg, are 0.0020, 0.0013, 0.0008, 0.0002 and 0.0001 respectively. Table II summarizes the scattering losses, probabilities of exceedance and the probabilities of encountering those losses associated with the most occurring fog events in the various cities in South Africa.

The Ijaz model in (6) and (8) is used to compute the atmospheric attenuation values for the wavelengths of 850 and 1550 nm. The most frequent fog events in the cities of Cape Town and Johannesburg have a visibility of 300 m. The probability of encountering and exceeding the scattering attenuations associated with the most frequent fog event in Cape Town is 0.0015 and 0.0042, respectively; while in Johannesburg, the probabilities of encountering and exceedance of the specific attenuations are 0.0008 and 0.0012, respectively. The most frequent fog events in Kimberley and Mbombela have visibilities of 800 m. However, the probabilities of exceedance and encountering of the scattering losses associated with the fog event is higher in Mbombela than in Kimberley.

Table III summarizes the specific attenuations, as well as the likelihoods of deceedance and encountering of such losses, aligned with the most frequent visibility measurements in the different cities of South Africa. The probability of deceedance describes the possibility of encountering values lesser than or equal to certain atmospheric attenuations. It enables the FSO system installer to also predict the link availability, once the most frequent and maximum atmospheric attenuations to be encountered by the link is known. Cape Town, Mbombela and Polokwane have the lowest probabilities of encountering attenuations associated with their most frequent visibility measurements. However, Polokwane has the least probability of deceedance when comparing the three cities. This implies that the probability of exceedance or encountering of attenuations greater than those associated with the most common visibility in Polokwane is 0.3619 or 36.19 % of the time investigated.

TABLE IV
COMMERCIAL FSO LINK PARAMETERS USED IN CALCULATIONS

Parameter	FSO Link A	FSO Link B
Wavelength (λ)	850 nm	1550 nm
Transmit Power (P_{Tx})	16 dBm	20 dBm
Receiver Sensitivity (R_s)	-38 dBm	-40 dBm
Transmitter (X_{Tx}) and Receiver (X_{Rx}) System Losses	2 dB	4 dB
Receiver Aperture Diameter (D)	16 cm	10 cm
Eye Safety	Class 1 M	Class 1 M
Receiver Field of View	10 mrad	65 mrad
Transmit Beam Divergence Angle (θ)	2.8 mrad	1.75 mrad
Responsivity $(\Re)$	0.4 A/W	0.5 A/W
Bit Rate (R_b)	1.25 Gb/s	10 Gb/s

IV. LINK BUDGET

The level of signal power detected at the receiver is determined by the link budget of an FSO link [24]. The average optical power detected at the receiver is given below as:

$$P_{Rx} \cong P_{Tx} - \beta_{sa}(\lambda)L - F_{SL} + G_{Tx} + G_{Rx} - L_{Geo} - X_{Tx} - X_{Rx} \quad (9)$$

where P_{Tx} is the power of the transmitted optical signal in dBm, β_{sa} is the aerosol scattering loss in dB/km, L is the propagation distance in km, F_{SL} is the free space path loss in dB, G_{Tx} is the gain of the transmit lens in dB, G_{Rx} is the gain of the receive lens in dB, L_{Geo} is the optical geometric loss in dB, X_{Tx} is the aggregate loss at the transmitter in dB and X_{Rx} is the aggregate loss at the receiver in dB. X_{Tx} and X_{Rx} include all other system-dependent losses such as beam direction misalignment, random changes in the beam centroid position and decrease in sensitivity as a result of background solar radiation [20].

The free space path loss is expressed as [25]-[26]:

$$F_{SL} = 20\log\left(\frac{4\pi L}{\lambda}\right) \quad (10)$$

where λ is transmit wavelength of the signal in metres. The gain of the transmit lens is derived below as [26]-[27]:

$$G_{Tx} = 20\log\left(\frac{126.491}{\theta}\right) \quad (11)$$

where θ is the transmit beam divergence angle in radians. The gain of the receive lens is expressed as [27]-[28]:

$$G_{Rx} = 20\log\left(\frac{31.623\pi D}{\lambda}\right) \quad (12)$$

where D is the diameter of the receiver aperture in metres. The geometric loss is caused by the optical beam diverging from its path. It is given as [28]-[29]:

$$L_{Geo} = -20\log\left(\frac{D}{L\theta}\right) \quad (13)$$

The optical link power margin determines how well a system compensates for atmospheric attenuation losses over a given propagation distance. It is the benchmark for assessing the performance of the FSO link, and is presented as [30]:

$$L_m(L) = P_{Tx} - X_{Tx} - 20\log\left(\frac{\theta L\sqrt{2}}{D}\right) - X_{Rx} - R_s \quad (14)$$

where R_s is the sensitivity of the receiver in dBm.

Commercial FSO link parameters used in this paper are shown in Table IV. In calculating the optical link margin, the constant parameters of the FSO links in Table IV are substituted into (14) which results in a simplified equation below:

$$L_m(L) = M_\circ - 20\log L \quad (15)$$

When the propagation distance, L, is in kilometres, the constant $M_\circ$ is equal to 24 dB when the parameters of the FSO link A are substituted into (14). This results in (16):

$$L_m(L)_{\text{Link A}} = 24 - 20\log L \quad (16)$$

When the parameters of FSO link B are substituted into (14), we have the simplified link margin equation for the FSO system transmitting at 1550 nm below:

$$L_m(L)_{\text{Link B}} = 28 - 20\log L \quad (17)$$

Some commercial FSO links currently manufactured, use 850 nm and 1550 nm wavelengths for signal transmission. In this work, the performance of two FSO links, labelled A and B are investigated. Typical FSO link parameters are shown in Table IV. Throughout this paper FSO link A transmits data signals on the 850 nm wavelength while FSO link B operates on the 1550 nm wavelength.

V. MINIMUM VISIBILITY

The minimum required visibility, $V_{\min}(L,V)$, must be determined for the FSO link to function optimally. It is a critical parameter for estimating the availability of an FSO link. It is presented in the form [16], [18]:

$$V \geq V_{\min}(L,V) \quad (18)$$

For a link to be available, the optical link margin must be greater than or equal to the atmospheric attenuation losses. That is [31]-[32]:

$$L_m(L) \geq A_\alpha(L,V) \quad (19)$$

The minimum required visibility, in kilometers, for the Ijaz and Kim models is given below as [16], [18]:

$$V_{\min}(L,V) = \frac{17L}{L_m(L)}\left(\frac{\lambda}{\lambda_\circ}\right)^{-q_\circ} \quad (20)$$

where the particle size distribution parameter, $q_\circ$, is presented for the Kim and Ijaz fog models in (7) and (8), respectively. Equation (18) therefore becomes:

$$V \geq \frac{17L}{L_m(L)}\left(\frac{\lambda}{\lambda_\circ}\right)^{-q_\circ} \quad (21)$$

Fig. 6 is generated using the Ijaz model shown in (8), (16), (17) and (21) during foggy periods. The parameters of the commercial FSO links shown in Table IV are used in the calculations as well. The minimum required visibility needed to achieve a link distance of 500 metres, is approximately 295 and 276 metres for the FSO links transmitting at a wavelength of 850 and 1550 nm, respectively.

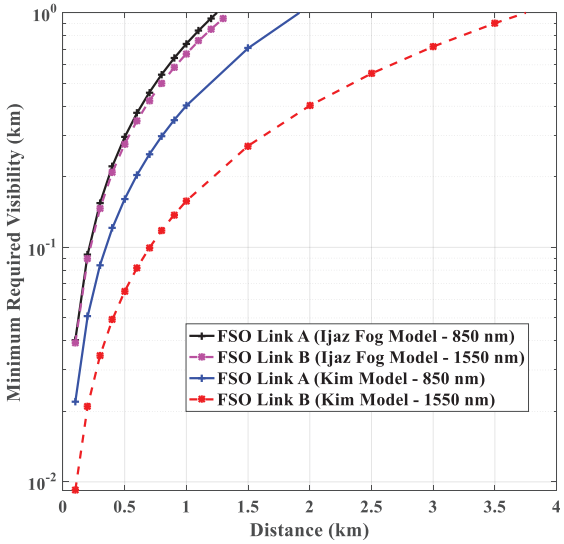

Fig. 6. Minimum required visibility vs link distance based on Ijaz and Kim models for FSO links A and B

The Kim model is used in computing the minimum required visibilities needed to achieve optimal link distances in Fig. 6 as well. Equations (7), (16), (17) and (21) are used in the computations of the minimum required visibilities during haze and clear weather periods. In order to achieve path lengths of 1.5 kilometres, the minimum required visibilities for FSO links transmitting at 850 and 1550 nm are 0.70 and 0.27 kilometres, respectively. It can be deduced from Fig. 6, that FSO links transmitting at 1550 nm achieve similar optimal link distances at lower minimum required visibilities than those transmitting at 850 nm.

A novel approach for estimating the availability of FSO links without the use of substantial visibility records is reported in [30], [32]. The cumulative distribution functions (CDF) of sample visibility data were fitted using the least squares third-order polynomial method. However, the approach used in [32] used only the Kim model for calculating the minimum required visibilities of FSO links transmitting at 850 nm from visibility data obtained from different airports across Europe.

Further research as reported in [17], [22], [23], propose that the Ijaz model is more accurate in computing aerosol scattering attenuation losses encountered by optical signals transmitting between wavelengths of 550 and 1600 nm for visibility measurements ranging from 15 to 1000 metres.

This necessitates the application of the Ijaz model in computing the CDFs of the minimum required visibilities and resultant link availabilities of FSO links during foggy weather. In this work, the same method implemented in [32] is also adopted, but only for estimating link availabilities of FSO links in clear weather, when visibility measurements are greater than 1 kilometer. The CDFs of minimum required visibilities during foggy weather are computed and the Ijaz model is used in estimating the availabilities of FSO links transmitting at 850 and 1550 nm in major cities of South Africa.

Similar to what was reported in [32], the third-order polynomial fitting method of the CDFs calculated, are a trade-off between simplicity and accuracy of the equations obtained.

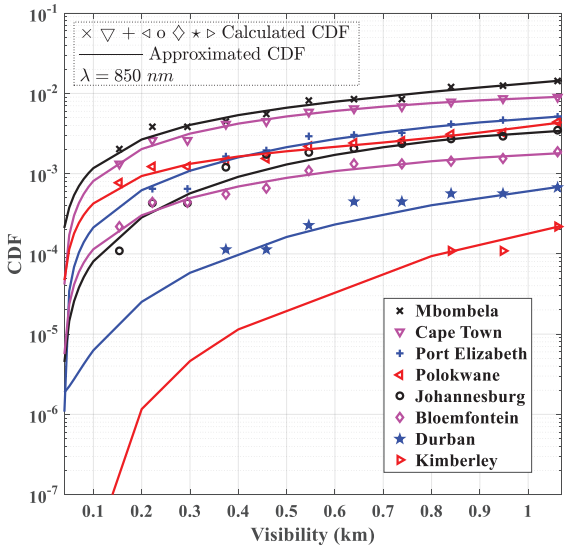

(a) 850 nm

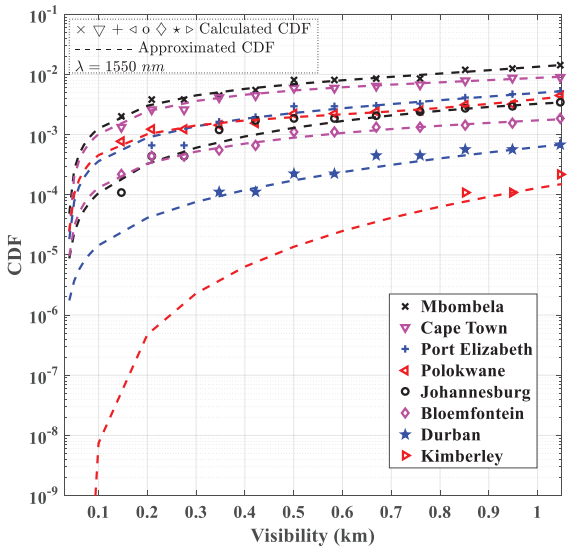

(b) 1550 nm

Fig. 7. Directly evaluated CDF and approximated CDF of fog for major cities in South Africa using Ijaz model for (a) 850 nm and (b) 1550 nm.

The higher-order (fourth to sixth) polynomials investigated did not necessarily improve the accuracy of the resultant availabilities calculated.

This is due to repetitive CDF values traceable to the approximation of the visibility data measured to just one decimal place. Therefore, the CDFs of the minimum required visibilities used in our computations is presented as:

$$F\left[V_{\min}\right] = \sum_{j=0}^{3} p_j V_{\min}^{j} \tag{22}$$

where p_j are the coefficients of the polynomial.

Tables V(a), V(b), VI(a) and VI(b) show the polynomial coefficients, error sum of squares (SSE), coefficient of determination (R^2) and the root mean square errors (RMSE) of fitted minimum required visibility CDFs during foggy and clear

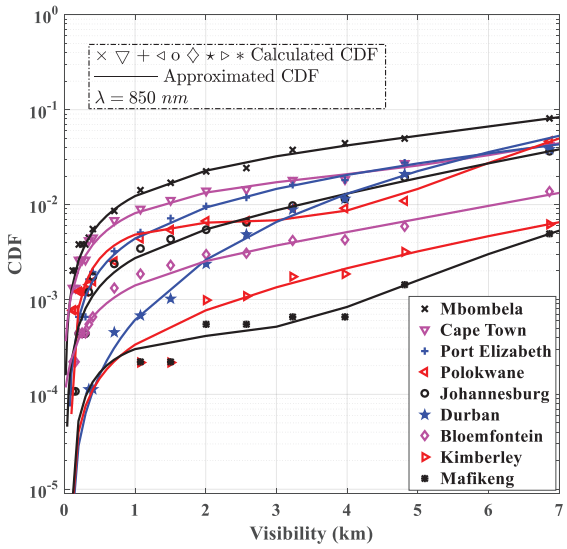

(a) 850 nm

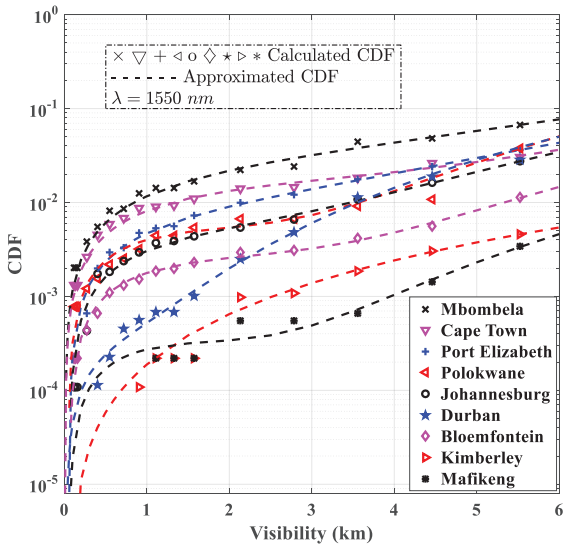

(b) 1550 nm

Fig. 8. Directly evaluated CDF and approximated CDF of minimum visibility for major cities in South Africa using Kim model for (a) 850 nm and (b) 1550 nm.

weather for transmission wavelengths of 850 and 1550 nm. It is clear from all the four tables that the directly calculated and the fitted minimum required visibility CDFs have relatively high R^2, and low SSEs and RMSEs not exceeding 0.1 and 1 metres during foggy and clear weather, respectively.

Figs. 7(a), 7(b), 8(a) and 8(b) show plots of directly evaluated and approximated minimum required visibility CDFs during foggy and clear weather for transmission wavelengths of 850 and 1550 nm. Inserting the values of the coefficients in Tables V(a), V(b), VI(a) and VI(b) into (22) yield plots of the approximated minimum required visibility CDFs in Figs. 7(a), 7(b), 8(a) and 8(b), respectively. Figs. 7(a) and (b) are based on the Ijaz fog model while Figs. 8(a) and (b) are calculated using the Kim model for both transmission wavelengths considered in this work. In Figs. 7(a) and 7(b), minimum visibility CDFs under fog conditions are presented. The plot for the city of Mafikeng is not shown because there were no fog events recorded in the data received from the SAWS over the time period investigated. In Figs. 8(a) and 8(b), minimum required visibility CDFs under fog and haze conditions are shown. All the four Figs. 7(a), 7(b), 8(a) and 8(b) show a high occurrence of minimum visibility under fog/haze conditions in the cities of Mbombela, Cape Town and Port Elizabeth for both transmission wavelengths considered. This clearly indicates that the FSO links in those cities will experience more scattering attenuation during data transmission and ultimately lower link availabilities as compared with the FSO links in the cities of Mafikeng and Kimberley which have very low occurrence of poor visibility events.

VI. Link Availability

The FSO link availability is majorly dependent on the atmospheric attenuation conditions. The availability of the two commercial FSO links based on the Ijaz and Kim models in this work is defined as [16], [18], [19], [30], 32]:

$$L_{Av} = \Pr obability\left[V \geq V_{\min}(L)\right] = 1 - F\left[V_{\min}(L)\right] \quad (23)$$

Figs. 9(a), 9(b), 10(a) and 10(b) show the directly evaluated link availabilities alongside the availabilities based on the calculations of approximated minimum required visibility CDFs during foggy and clear weather conditions in different cities of South Africa. It is quite evident from the four figures that Mafikeng, Kimberley and Durban have link availabilities of almost 100% over all the propagation distances considered. This is because of the relatively high visibility measurements as well as the rare occurrence of fog events in those places as shown in Table III. Relatively low availability performance is seen in Port Elizabeth, Cape Town and Mbombela due to unstable weather conditions and relatively high occurrence of fog events in those locations. The link availability reduces with increase in the propagation distance between the two FSO transceivers. In comparison with the 850 nm wavelength, optical signals transmitted at 1550 nm have better availability performance over specific propagation distance in all the cities investigated.

VII. Signal to Noise Ratio (SNR), Bit Error Rate (BER) and Data Rate Estimation

Regardless of the length of propagation distance, the optical signal still suffers from random amplitude fluctuations, or scintillation effect, when it passes through the free-space channel. This is due to atmospheric turbulence which is mostly caused by small-scale temperature changes in the atmosphere, which induce variations in the refractive index. As a result of the amplitude fluctuations in the received signal, the BER increases, thus degrading the performance of the system [34]. The lognormal distribution is generally preferred in characterizing the received intensity, I, in a weak turbulence regime. Foggy weather is usually accompanied with weak turbulence as fog does not occur under direct sunshine [35]. The probability distribution function (PDF) of a lognormal variable I with small variance is given in [36] as:

TABLE V (a)
POLYNOMIAL COEFFICIENTS OF FITTED MINIMUM REQUIRED VISIBILITY CDFS CALCULATED FOR MAJOR CITIES IN SOUTH AFRICA DURING FOGGY WEATHER AND AT TRANSMISSION WAVELENGTHS OF 850 nm

		Coefficients of p_j				Tests		
Location	Range (km)	p_3	p_2	p_1	p_0	SSE	R^2	RMSE
Mbombela	0.04<V<1	5.02×10^{-3}	-8.26×10^{-3}	1.71×10^{-2}	-4.55×10^{-4}	5.17×10^{-6}	0.979	6.86×10^{-4}
Cape Town		9.41×10^{-5}	-4.26×10^{-3}	1.34×10^{-2}	-4.88×10^{-4}	1.06×10^{-6}	0.990	3.10×10^{-4}
Port Elizabeth		-2.16×10^{-3}	4.15×10^{-3}	2.99×10^{-3}	-1.25×10^{-4}	6.23×10^{-7}	0.983	2.38×10^{-4}
Polokwane		6.14×10^{-3}	-9.61×10^{-3}	7.55×10^{-3}	-2.40×10^{-4}	4.04×10^{-7}	0.978	1.92×10^{-4}
Johannesburg		-3.09×10^{-3}	5.85×10^{-3}	5.00×10^{-4}	-2.47×10^{-5}	5.69×10^{-7}	0.967	2.27×10^{-4}
Bloemfontein		-5.70×10^{-4}	6.21×10^{-4}	1.73×10^{-3}	-6.47×10^{-5}	1.09×10^{-7}	0.975	9.96×10^{-5}
Durban		-1.28×10^{-4}	7.71×10^{-4}	-3.26×10^{-5}	1.95×10^{-6}	3.89×10^{-8}	0.937	5.94×10^{-5}
Kimberley		1.78×10^{-4}	8.96×10^{-6}	-3.70×10^{-6}	1.23×10^{-7}	7.01×10^{-9}	0.880	2.52×10^{-5}

TABLE V (b)
POLYNOMIAL COEFFICIENTS OF FITTED MINIMUM REQUIRED VISIBILITY CDFS CALCULATED FOR MAJOR CITIES IN SOUTH AFRICA DURING FOGGY WEATHER AND AT TRANSMISSION WAVELENGTHS OF 1550 nm.

		Coefficients of p_j				Test		
Location	Range (km)	p_3	p_2	p_1	p_0	SSE	R^2	RMSE
Mbombela	0.04<V<1	1.28×10^{-2}	-2.17×10^{-2}	2.31×10^{-2}	-8.42×10^{-4}	6.08×10^{-6}	0.975	7.12×10^{-4}
Cape Town		7.73×10^{-3}	-1.71×10^{-2}	1.89×10^{-2}	-7.04×10^{-4}	1.31×10^{-6}	0.988	3.31×10^{-4}
Port Elizabeth		2.60×10^{-3}	-3.65×10^{-3}	6.19×10^{-3}	-2.24×10^{-4}	1.07×10^{-6}	0.969	2.99×10^{-4}
Polokwane		7.95×10^{-3}	-1.26×10^{-2}	8.82×10^{-3}	-3.08×10^{-4}	4.11×10^{-7}	0.978	1.85×10^{-4}
Johannesburg		-1.93×10^{-3}	4.13×10^{-3}	1.09×10^{-3}	-4.12×10^{-5}	8.71×10^{-7}	0.949	2.69×10^{-4}
Bloemfontein		5.04×10^{-5}	-3.28×10^{-4}	2.07×10^{-3}	-7.29×10^{-5}	1.09×10^{-7}	0.975	9.53×10^{-5}
Durban		1.55×10^{-4}	3.05×10^{-4}	1.66×10^{-4}	-5.39×10^{-6}	3.29×10^{-8}	0.947	5.23×10^{-5}
Kimberley		1.51×10^{-4}	-2.30×10^{-5}	9.91×10^{-7}	-1.26×10^{-8}	3.85×10^{-9}	0.867	1.79×10^{-5}

TABLE VI (a)
POLYNOMIAL COEFFICIENTS OF FITTED MINIMUM REQUIRED VISIBILITY CDFS CALCULATED FOR MAJOR CITIES IN SOUTH AFRICA DURING CLEAR WEATHER AND AT TRANSMISSION WAVELENGTHS OF 850 nm.

		Coefficients of p_j				Tests		
Location	Range (km)	p_3	p_2	p_1	p_0	SSE	R^2	RMSE
Mbombela	0.1<V<7	1.82×10^{-4}	-1.53×10^{-3}	1.38×10^{-2}	-1.16×10^{-4}	4.17×10^{-5}	0.995	1.57×10^{-3}
Polokwane		4.49×10^{-4}	-3.32×10^{-3}	8.44×10^{-3}	-7.49×10^{-4}	1.33×10^{-5}	0.993	8.85×10^{-4}
Johannesburg		9.50×10^{-5}	-3.17×10^{-4}	3.02×10^{-3}	-7.48×10^{-5}	6.02×10^{-6}	0.996	5.95×10^{-4}
Durban		9.42×10^{-5}	4.07×10^{-4}	1.21×10^{-4}	-1.26×10^{-5}	5.05×10^{-5}	0.981	1.72×10^{-3}
Cape Town		2.16×10^{-4}	-2.00×10^{-3}	9.74×10^{-3}	1.69×10^{-4}	1.84×10^{-5}	0.992	1.04×10^{-3}
Port Elizabeth		2.60×10^{-5}	4.73×10^{-5}	4.60×10^{-3}	-2.94×10^{-4}	9.52×10^{-6}	0.996	7.48×10^{-4}
Bloemfontein		3.76×10^{-5}	-2.07×10^{-4}	1.49×10^{-3}	8.86×10^{-5}	2.33×10^{-6}	0.987	3.70×10^{-4}
Mafikeng		3.73×10^{-5}	-2.28×10^{-4}	5.37×10^{-4}	-4.62×10^{-5}	1.61×10^{-7}	0.993	9.73×10^{-5}
Kimberley		1.21×10^{-5}	-1.90×10^{-6}	3.55×10^{-4}	-3.10×10^{-5}	3.55×10^{-7}	0.992	1.44×10^{-4}

TABLE VI (b)
POLYNOMIAL COEFFICIENTS OF FITTED MINIMUM REQUIRED VISIBILITY CDFS CALCULATED FOR MAJOR CITIES IN SOUTH AFRICA DURING CLEAR WEATHER AND AT TRANSMISSION WAVELENGTHS OF 1550 nm.

		Coefficients of p_j				Tests		
Location	Range (km)	p_3	p_2	p_1	p_0	SSE	R^2	RMSE
Mbombela		2.54×10^{-4}	-1.57×10^{-3}	1.31×10^{-2}	-1.26×10^{-4}	8.15×10^{-5}	0.988	1.97×10^{-3}
Polokwane		5.76×10^{-4}	-3.20×10^{-3}	6.96×10^{-3}	-3.41×10^{-4}	5.64×10^{-5}	0.963	1.64×10^{-3}
Johannesburg		2.55×10^{-4}	-1.29×10^{-3}	4.35×10^{-3}	-2.71×10^{-4}	1.67×10^{-6}	0.998	2.82×10^{-4}
Durban		2.75×10^{-4}	-3.57×10^{-4}	6.18×10^{-4}	-1.42×10^{-5}	4.08×10^{-5}	0.977	1.39×10^{-3}
Cape Town	$0.1<V<6$	2.75×10^{-4}	-2.35×10^{-3}	1.03×10^{-2}	-8.51×10^{-5}	1.76×10^{-5}	0.989	9.17×10^{-4}
Port Elizabeth		1.97×10^{-4}	-9.32×10^{-4}	5.76×10^{-3}	-3.34×10^{-4}	2.61×10^{-6}	0.999	3.53×10^{-4}
Bloemfontein		1.71×10^{-4}	-1.09×10^{-3}	2.88×10^{-3}	-1.78×10^{-4}	5.50×10^{-7}	0.996	1.62×10^{-4}
Mafikeng		5.30×10^{-5}	-2.77×10^{-4}	5.28×10^{-4}	-3.09×10^{-5}	2.15×10^{-7}	0.982	1.01×10^{-4}
Kimberley		2.52×10^{-6}	1.24×10^{-4}	6.99×10^{-5}	-8.08×10^{-6}	1.43×10^{-7}	0.995	8.26×10^{-5}

TABLE VII
WIND VELOCITIES (W_S), ALTITUDES AND REFRACTIVE INDEXES [33].

City	Average W_s (m/s)	Altitude (m)	Refractive Index ($m^{-2/3}$)
Kimberley	4.10	1196	2.4629×10^{-13}
Mafikeng	3.96	1281	2.0566×10^{-13}
Johannesburg	4.18	1695	1.9574×10^{-13}
Mbombela	2.82	865	5.5406×10^{-14}
Polokwane	2.82	1226	5.4351×10^{-14}
Bloemfontein	2.45	1354	2.9039×10^{-14}
Port Elizabeth	5.41	69	2.3653×10^{-14}
Durban	3.47	106	8.7979×10^{-15}
Cape Town	5.14	42	7.5257×10^{-15}

$$p(I)=\frac{1}{I\sqrt{2\pi\sigma_{SI}^2}}\exp\left\{-\left(\frac{In(I)+\frac{\sigma_{SI}^2}{2}}{\sqrt{2\sigma_{SI}^2}}\right)^2\right\} \tag{24}$$

where σ_{SI}^2 is the scintillation index parameter that indicates the amount of scintillation in the atmosphere. Based on the zero inner scale model, the scintillation index is expressed in [37]-[38] as:

$$\sigma_{SI}^2=\exp\left[\frac{0.49\sigma_{sw}^2}{\left(1+0.18d_s^2+0.56\sigma_{sw}^{12/5}\right)^{7/6}}+\frac{0.51\sigma_{sw}^2\left(1+0.69\sigma_{sw}^{12/5}\right)^{-5/6}}{1+0.90d_s^2+0.62d_s^2\sigma_{sw}^{12/5}}\right]-1 \tag{25}$$

where $\sigma_{sw}^2=0.50C_n^2\left(\sqrt[6]{k^7L^{11}}\right)$ is the Rytov variance for the spherical wave, $d_s=\sqrt{\frac{kD^2}{4L}}$, C_n^2 is the refractive index structure parameter in $m^{-2/3}$, and $k=\frac{2\pi}{\lambda}$ is the wave number in m^{-1}. In weak turbulence conditions, σ_{SI}^2 is less than unity [37]. For optical spherical waves, the scintillation indices of all the locations considered in South Africa based on the average parameters shown in Table VII were also less than unity [33].

Most commercial FSO links on the market are still using intensity modulation/direct detection (IM/DD) schemes for operation. The performance of non-return-to-zero on-off keying (NRZ-OOK) modulation scheme and avalanche photodiode (APD) FSO systems are investigated in this section. The total APD receiver noise mainly consists of the shot noise σ_{Sh}^2, and thermal noise σ_{Th}^2. It is expressed in [39] as:

$$\sigma_N^2=\sigma_{Th}^2+\sigma_{Sh}^2 \tag{26}$$

Thermal noise arises as a result of current fluctuation caused by the thermal motion of electrons at some finite temperature, even when there is no signal transmission. It is given in [40] as:

$$\sigma_{Th}^2=\frac{2TK_BR_bF_n}{R} \tag{27}$$

where T is the receiver temperature, K_B is the Boltzmann constant, R_b is the bit rate, F_n is the amplifier noise figure and R is the APD load resistance. The shot noise is also denoted in [40] as:

$$\sigma_{Sh}^2=2qg^2\Re F_AR_bP_{Rx}I+\sigma_{Th}^2 \tag{28}$$

where q is the charge of an electron, g is the APD gain, $\Re$ is the responsivity, P_{Rx} is the power of the received signal and F_A is the excess noise factor.

F_A is expressed as:

$$F_A=k_Ag+\left(1-k_A\right)\left(2-g^{-1}\right) \tag{29}$$

where k_A is the ionization factor.

The instantaneous SNR (γ_o) at the receiver is given as:

$$\gamma_o=\frac{\left(2g\Re P_{Rx}I\right)^2}{\sigma_N^2} \tag{30}$$

The conditional BER of the FSO communication system employing IM/DD and based on the NRZ-OOK modulation scheme is given by [41]:

$$BER=\frac{1}{2}erfc\left(\frac{\sqrt{\gamma_o}}{2\sqrt{2}}\right)=Q\left(\frac{\sqrt{\gamma_o}}{2}\right) \tag{31}$$

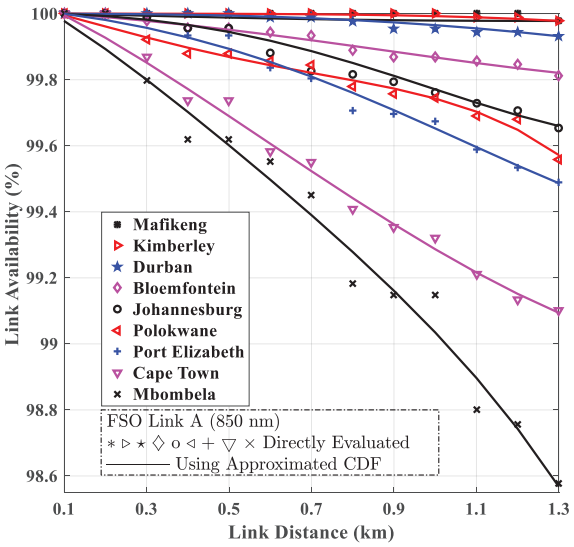

(a) 850 nm

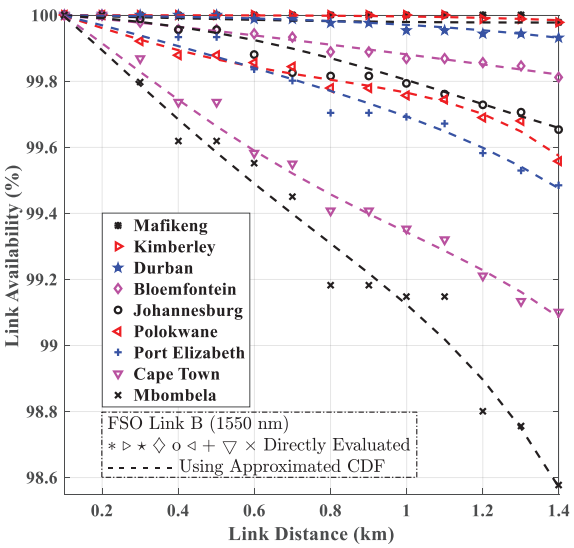

(b) 1550 nm

Fig. 9. Link availability for commercial FSO links for various cities in South Africa during foggy periods using Ijaz's model for (a) 850 nm and (b) 1550 nm.

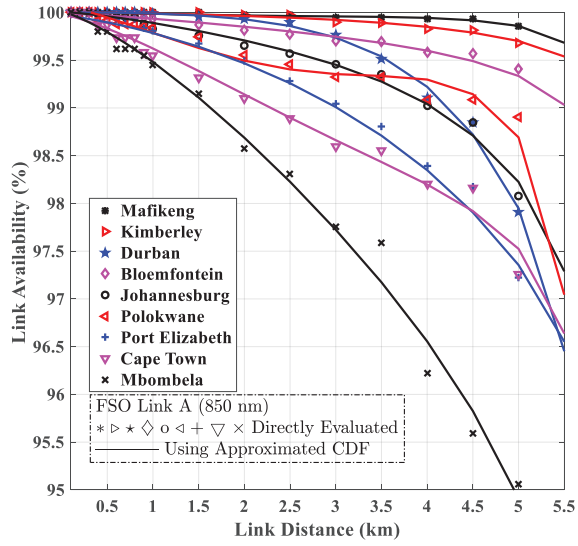

(a) 850 nm

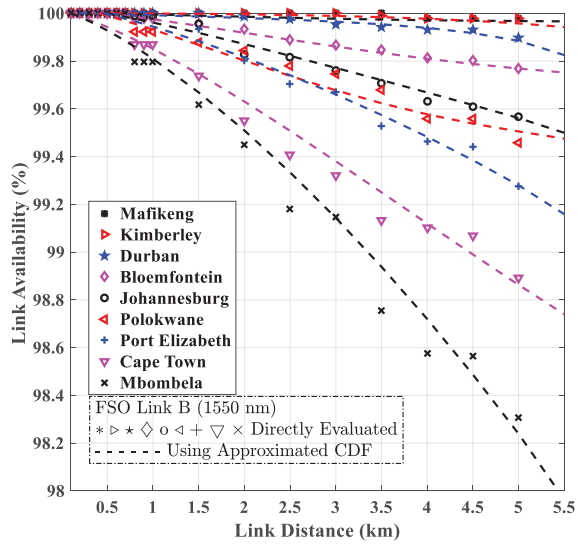

(b) 1550 nm

Fig. 10. Link availability based on the Kim model for commercial FSO links during clear weather conditions for various cities in South Africa for (a) 850 nm and (b) 1550 nm.

Substituting (30) into (31), yields:

$$BER = \frac{1}{2} erfc\left(\frac{2g\Re P_{Rx} I}{2\sqrt{2}\left(\sqrt{\sigma_N^2}\right)}\right) \tag{32}$$

Equation (32) represents the conditional BER in a turbulence-free channel. Taking into account the effect of weak atmospheric turbulence on (32), the average BER over the lognormal fading channel is obtained by averaging (31) over (24):

$$BER = \int_0^\infty Q\left(\frac{\sqrt{\gamma_o}}{2}\right).p(I)dI \tag{33}$$

Employing the change of variable, z, we have:

$$z = \frac{In(I) + \frac{\sigma_{SI}^2}{2}}{\sqrt{2\sigma_{SI}^2}} \tag{34}$$

Making I the subject of (34), we obtain:

$$I = \exp\left(z\sqrt{2\sigma_{SI}^2} - \frac{\sigma_{SI}^2}{2}\right) \tag{35}$$

Differentiating I with respect to z, we have:

$$dI = \sqrt{2\sigma_{SI}^2}\exp\left(z\sqrt{2\sigma_{SI}^2} - \frac{\sigma_{SI}^2}{2}\right)dz \tag{36}$$

Substituting (24), (34), (35) and (36) into (33), we obtain:

TABLE VIII
FSO LINK PARAMETERS FOR SNR, BER AND DATA RATE

Parameter	Values
Light Source	Laser
Boltzmann's constant (K_B)	1.381×10^{-23} J/K
Temperature (T)	298 K
Transmitter efficiency (τ_{Tx})	80 %
Receiver efficiency (τ_{Rx})	80 %
Planck's constant (h)	6.626×10^{-34} Js
Speed of light (c)	3×10^{8} m/s
Detector	Avalanche Photodiode (APD)
APD Load Resistance (R)	1000 Ω
APD gain (g)	50
Amplifier noise figure (F_n)	2
Charge of an electron (q)	1.6022×10^{-19} C
Ionization factor for (InGaAs APD) (k_A)	0.7

$$BER = \frac{1}{\sqrt{\pi}} \int_0^{\infty} Q\left(\frac{\sqrt{\gamma_o}}{2}\right) \exp\left(-z^2\right) dz \tag{37}$$

Further substitution of (27), (28), (30), (32) and (35) into (37) yields:

$$BER = \frac{1}{2\sqrt{\pi}} \bullet \int_0^{\infty} erfc \left(\frac{2g\Re P_{Rx}.\exp\left(z\sqrt{2\sigma_{SI}^2} - \frac{\sigma_{SI}^2}{2}\right)}{2\sqrt{2}} \bullet \frac{1}{\left(\sqrt{\sigma_{Th}^2} + \sqrt{2qg^2\Re F_A R_b P_{Rx}.\exp\left(z\sqrt{2\sigma_{SI}^2} - \frac{\sigma_{SI}^2}{2}\right) + \sigma_{Th}^2}\right)} \right) \bullet \exp\left(-z^2\right) dz \tag{38}$$

Equation (38) can be evaluated using the Gauss-Hermite approximation as presented in [42]-[43] as:

$$\int_{-\infty}^{\infty} \exp\left(-x^2\right) f(x) dx \cong \sum_{i=1}^{n} w_i f(z_i) \tag{39}$$

where

$$f(z) = erfc \left(\frac{g\Re P_{Rx}.\exp\left(z\sqrt{2\sigma_{SI}^2} - \frac{\sigma_{SI}^2}{2}\right)}{\sqrt{2}} \bullet \frac{1}{\left(\sqrt{\sigma_{Th}^2} + \sqrt{2qg^2\Re F_A R_b P_{Rx}.\exp\left(z\sqrt{2\sigma_{SI}^2} - \frac{\sigma_{SI}^2}{2}\right) + \sigma_{Th}^2}\right)} \right) \tag{40}$$

Equation (39) thus becomes:

$$BER \cong \frac{1}{2\sqrt{\pi}} \sum_{i=1}^{n} w_i \bullet \left(erfc \left(\frac{g\Re P_{Rx}.\exp\left(z\sqrt{2\sigma_{SI}^2} - \frac{\sigma_{SI}^2}{2}\right)}{\sqrt{2}} \bullet \frac{1}{\left(\sqrt{\sigma_{Th}^2} + \sqrt{2qg^2\Re F_A R_b P_{Rx}.\exp\left(z\sqrt{2\sigma_{SI}^2} - \frac{\sigma_{SI}^2}{2}\right) + \sigma_{Th}^2}\right)} \right) \right) \tag{41}$$

where the values of the weights, w_i and zeros of the Hermite polynomial, z_i, are given in [42]-[43].

The achievable data rate, R_D, of an FSO link is given in [44] as:

$$R_D = \frac{P_{Tx}\tau_{Tx}\tau_{Rx}A_{Rx}}{\pi(0.5\theta)^2 L^2 E_p N_b A_\alpha F_{SL} L_{Geo}} \tag{42}$$

where τ_{Tx} is the transmitter efficiency, τ_{Rx} is the receiver efficiency, A_{Rx} is the area of the receiver lens, N_b is the receiver sensitivity, $E_p = \frac{hc}{\lambda}$ is the energy of the photon, h is Planck's constant and c is the speed of light.

The receive SNR for commercial FSO links A and B over link distances for the most frequent fog conditions peculiar to each of the various cities of South Africa are presented in Figs. 11(a) and (b), respectively. The numerical results are derived from parameters in Tables II, IV and VIII as well as (26) to (30). It is evident from Figs. 11 (a) and (b) that the FSO links in the cities of Cape Town and Johannesburg will have the lowest link performance due to the occurrence of thick fog events. For a receive SNR of 20 dB, both links have the least propagation distance of about 600 – 680 metres with FSO link B slightly out-performing the FSO link A due to their transmission wavelength. FSO links in the city of Mafikeng have improved performance due to the occurrence of only very light fog weather as compared with other cities in South Africa.

Figs. 12(a) and (b) show the SNRs needed to achieve certain BERs for single-input single-output (SISO) FSO links A and B in various cities of South Africa. The numerical results are calculated from parameters in (41) and Tables II, IV, VII, and VIII. The FSO links in the cities of Mafikeng and Kimberley require more power to achieve lower BERs than other cities in South Africa. In Fig. 12(a), to achieve a BER of 10^{-4}, the FSO links in Mafikeng and Kimberley require an SNR of ~48.5 dB while the links in other cities require less than 48 dB to achieve the same BER. A similar performance is seen in Fig. 12(b). The poorer BER performances of FSO links in Mafikeng and Kimberley are caused by high wind speeds, refractive indexes and altitudes as compared with other cities of South Africa. This is highlighted in Table VII as shown in [33].

Figs. 13(a) and (b) show the BER performance of FSO links over propagation distances in the various cities of South Africa. Of all the propagation path lengths considered, the FSO links in Mafikeng and Mbombela have better performances than those in the other cities considered.

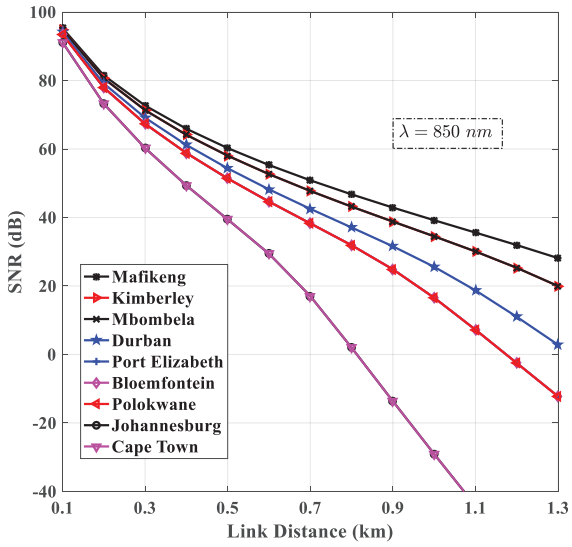

(a) 850 nm

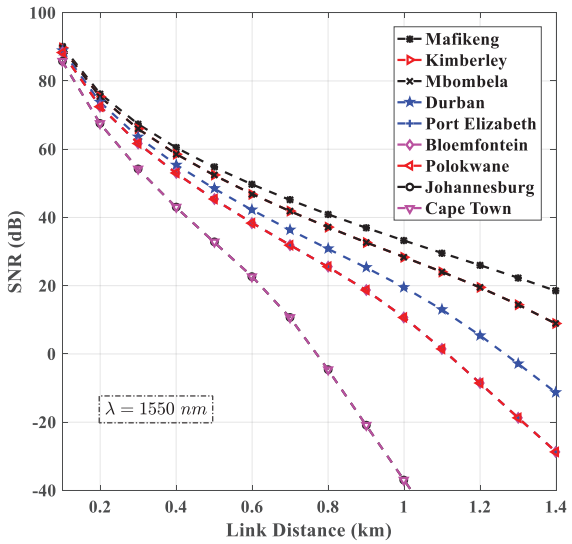

(b) 1550 nm

Fig. 11. Receive SNR for commercial FSO link for various cities in South Africa during foggy periods for (a) 850 nm and (b) 1550 nm.

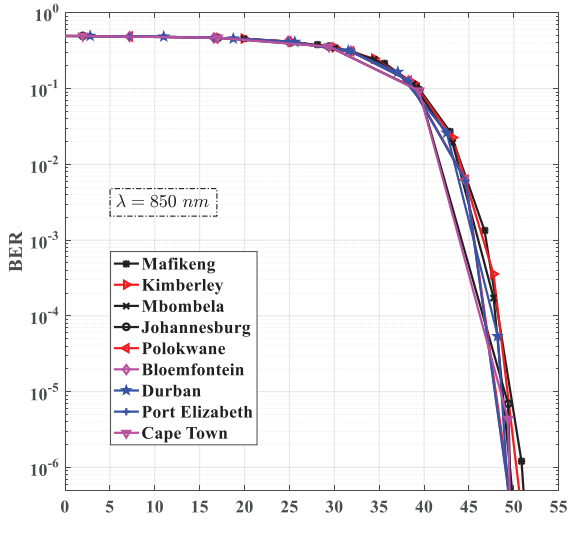

(a) 850 nm

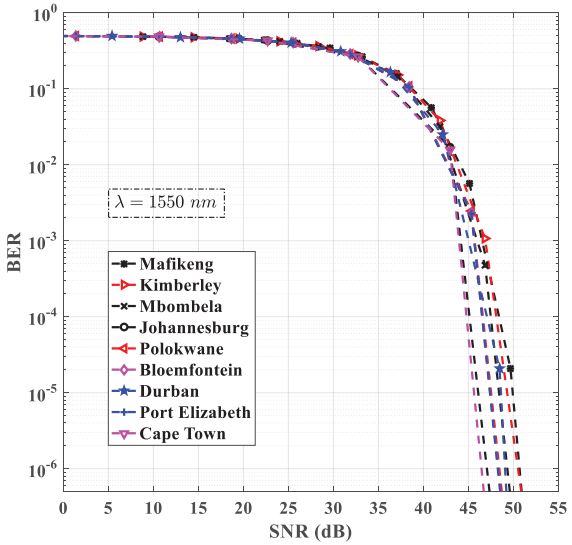

(b) 1550 nm

Fig. 12. BER of SISO FSO links employing OOK modulation during foggy weather and weak atmospheric turbulence for (a) 850 nm and (b) 1550 nm.

In Fig. 13(a), a BER of 10^{-4} is achieved over a link distance of 760 metres in Mafikeng, while the same BER can only be achieved over a path length of 415 metres in Cape Town. Similarly, to obtain a BER of 10^{-6} in Fig. 13(b), link distances of not more than 580 metres and 370 metres will attain the BER performance in Mafikeng and Cape Town, respectively.

The highest data rates over link distances that can be achieved by FSO systems under foggy weather conditions in various cities of South Africa are shown in Figs. 14(a) and (b). These numerical results are calculated from (42) and parameters in Tables II, IV and VIII. FSO links transmitting at 1550 nm achieve higher data rates than the 850 nm links. It is evident from both figures that the aerosol scattering attenuation due to fog greatly impacts data transmission rates.

The FSO links in Johannesburg and Cape Town have the lowest data rates performance over the link distances considered during their most occurring dense fog event. The cities of Mafikeng, Kimberley and Mbombela have better data transmission rates due to very light fog events that occur in those locations.

VIII. CONCLUSION

In this paper, availability analysis of terrestrial FSO communication links based on the climatic peculiarities of various cities in South Africa are presented. Cumulative distributions of aerosol scattering attenuation based on Kim and Ijaz models were carried out using visibility data for the locations of interest. Probabilities of exceedance, deceedance and encountering of scattering attenuation is shown.

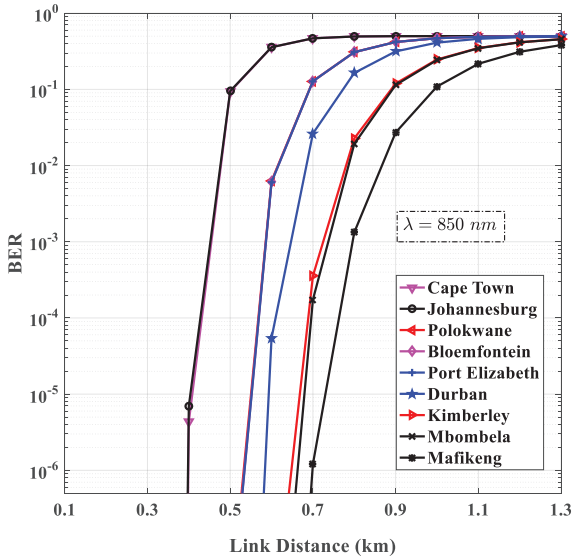

(a) 850 nm

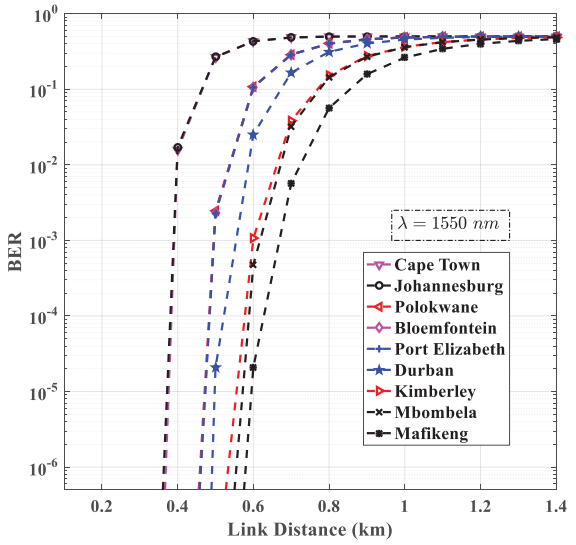

(b) 1550 nm

Fig. 13. BER performance of SISO FSO links employing OOK modulation over link distances in a foggy and weak turbulence regime for (a) 850 nm and (b) 1550 nm.

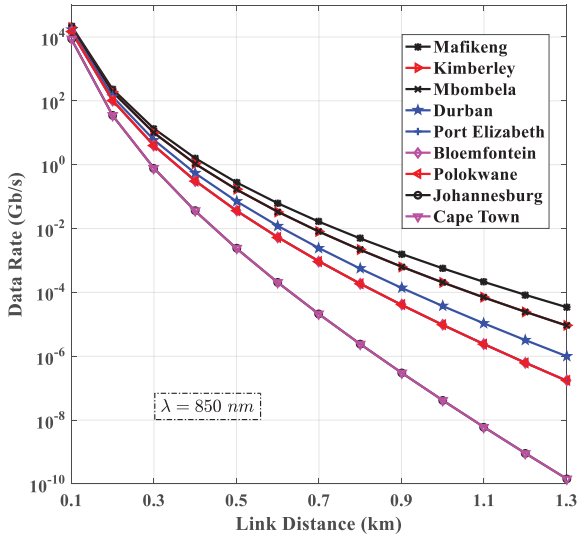

(a) 850 nm

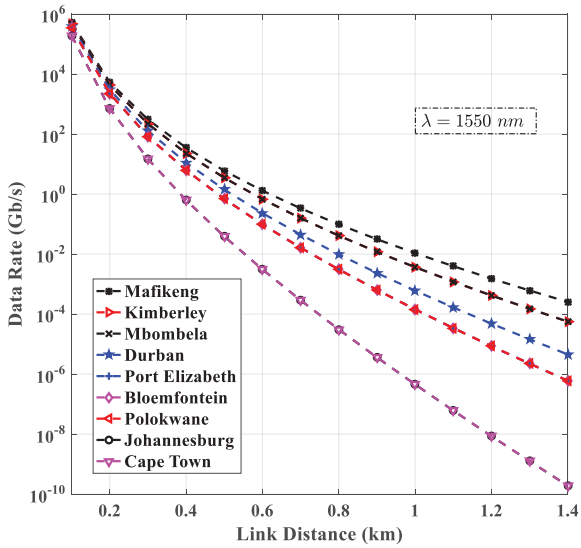

(b) 1550 nm

Fig. 14. Attainable data rates of horizontal FSO links over link distances under foggy weather conditions for (a) 850 nm and (b) 1550 nm.

Link budget analysis for two FSO links transmitting at two wavelengths were carried out. The resultant link margin equations derived were implemented in evaluating minimum required visibilities for two links in foggy and clear weather conditions. Approximate polynomial equations for calculating the minimum required visibilities for all the cities considered are derived, and then applied in estimating link availabilities of two commercial FSO links. Plots of the receive SNR and data rate performance in foggy weather conditions are presented. BER and link performance plots are presented for two links in the presence of weak atmospheric turbulence based on average weather parameters of several cities of South Africa. The FSO system transmitting at 1550 nm is seen to outperform the one transmitting at 850 nm based on all the performance metrics used. This work may be extended in future by investigating different localized climatic constraints on the various types of optical signals such as plane, spherical and Gaussian beam waves. This would aid in the modeling of different types of attenuations for locations of interest where FSO or hybrid FSO systems are to be deployed.

IX. ACKNOWLEDGEMENT

The authors of this paper would like to express their gratitude to the South African Weather Service (SAWS) for providing the data used in this work.

X. REFERENCES

[1] S. Chauhan, R. Miglani, L. Kansal, G. S. Gaba, and M. Masud, "Performance Analysis and Enhancement of Free Space Optical Links for Developing State-of-the-Art Smart City Framework," *Photonics*, vol. 7, no. 4, p. 132, Dec. 2020, DOI: 10.3390/photonics7040132.

[2] M. Fuentes, J. L. Carcel, C. Dietrich, L. Yu, E. Garro, V. Pauli, *et al.*, "5G new radio evaluation against IMT-2020 key performance indicators," *IEEE Access,* vol. 8, pp. 110880-110896, 2020, DOI: 10.1109/ACCESS.2020.3001641.

[3] J. Kim, J. Song, W. Seo, I. Ihm, S.-H. Yoon, and S. Park, "XR Framework for Collaborating Remote Heterogeneous Devices," *2020 IEEE Conference on Virtual Reality and 3D User Interfaces Abstracts and Workshops (VRW)*, 2020, pp. 587-588, DOI: 10.1109/VRW50115.2020.00144.

[4] S. Böcker, C. Arendt, P. Jörke, and C. Wietfeld, "LPWAN in the Context of 5G: Capability of LoRaWAN to Contribute to mMTC," *2019 IEEE 5th World Forum on Internet of Things (WF-IoT)*, 2019, pp. 737-742, DOI: 10.1109/WF-IoT.2019.8767333.

[5] M. Garlinska, A. Pregowska, K. Masztalerz, and M. Osial, "From Mirrors to Free-Space Optical Communication—Historical Aspects in Data Transmission," *Future Internet,* vol. 12, no. 11, p. 179, Oct. 2020, DOI: 10.3390/fi12110179.

[6] B. Bag, A. Das, I. S. Ansari, A. Prokeš, C. Bose, and A. Chandra, "Performance analysis of hybrid FSO systems using FSO/RF-FSO link adaptation," *IEEE Photonics Journal,* vol. 10, no. 3, pp. 1-17, June 2018, DOI: 10.1109/JPHOT.2018.2837356.

[7] S. Malik and P. K. Sahu, "Free space optics/millimeter-wave based vertical and horizontal terrestrial backhaul network for 5G," *Optics Communications,* vol. 459, p. 125010, Mar. 2020, DOI: 10.1016/j.optcom.2019.125010.

[8] C. J. Engelbrecht and F. A. Engelbrecht, "Shifts in Köppen-Geiger climate zones over southern Africa in relation to key global temperature goals," *Theoretical and applied climatology,* vol. 123, pp. 247-261, 2016, DOI: 10.1007/s00704-014-1354-1.

[9] P. D. Tyson and R. A. Preston-Whyte, "Atmospheric circulation and weather over southern africa," in *Weather and climate of southern Africa*, 2nd ed. Cape Town, South Africa: Oxford University Press Southern Africa, 2000, ch. 12, pp. 176-217.

[10] M. O. Odedina, "A semi-empirical formulation for determination of rain attenuation on terrestrial radio links," Ph.D. dissertation, Sch. Elect. Electron. Comp. Eng., Univ. KwaZulu-Natal, Durban, South Africa, 2010.

[11] P. A. Owolawi, "Characteristics of rain at microwave and millimetric bands for terrestrial and satellite links attenuation in South Africa and surrounding islands," Ph.D. dissertation, Sch. Elect. Electron. Comp. Eng., Univ. KwaZulu-Natal, Durban, South Africa, 2010.

[12] M. Tadross and P. Johnston, , "Climate systems regional report: Southern Africa," ICLEI–Local Governments for Sustainability–Africa, Cape Town, South Africa, 105868-001, Aug. 2012, [Online]. Available: https://idl-bnc-idrc.dspacedirect.org/bitstream/handle/10625/50398/IDL-50398.pdf?sequence=1&isAllowed=y.

[13] O. O. Kolawole, M. Mosalaosi, and T. J. Afullo, "Visibility modeling and prediction for free space optical communication systems for South Africa," *International Journal on Communications Antenna and Propagation,* vol. 10, no. 3, pp. 161-174, 2020, DOI: 10.15866/irecap.v10i3.18008.

[14] K. Dev, R. Nebuloni, and C. Capsoni, "Optical attenuation measurements in low visibility conditions," *2016 10th European Conference on Antennas and Propagation (EuCAP)*, 2016, pp. 1-5, DOI: 10.1109/EuCAP.2016.7481270.

[15] V. Kvicera, M. Grabner, and J. Vasicek, "Assessing availability performances of free space optical links from airport visibility data," *2010 7th International Symposium on Communication Systems, Networks & Digital Signal Processing (CSNDSP 2010)*, 2010, pp. 562-565, DOI: 10.1109/CSNDSP16145.2010.5580372.

[16] O. Kolawole, T. Afullo, and M. Mosalaosi, "Estimation of Optical Wireless Communication Link Availability Using Meteorological Visibility Data for Major Locations in South Africa," *2019 PhotonIcs & Electromagnetics Research Symposium-Spring (PIERS-Spring)*, 2019, pp. 319-325, DOI: 10.1109/PIERS-Spring46901.2019.9017842.

[17] M. M. Shumani, M. Abdullah, and A. Basahel, "Availability analysis of terrestrial free space optical (FSO) link using visibility data measured in tropical region," *Optik,* vol. 158, pp. 105-111, April 2018, DOI: 10.1016/j.ijleo.2017.11.203.

[18] O. O. Kolawole, "Performance analysis of optical wireless communication systems in a warm-summer Mediterranean climatic region," M.S. thesis, Sch. Elect. Electron. Comp. Eng., Univ. KwaZulu-Natal, Durban, South Africa, 2017.

[19] J. Mohale, M. R. Handura, T. O. Olwal, and C. N. Nyirenda, "Feasibility study of free-space optical communication for South Africa," *Optical Engineering,* vol. 55, no. 5, p. 056108, May 2016, DOI: 10.1117/1.OE.55.5.056108.

[20] P. Anokye, "Free space optical communication over the Ghanaian Turbulent Atmospheric Channel," M.S. thesis, Dept. Elect. Electron. Eng., Kwame Nkrumah Univ. Sci. Tech., Kumasi, Ghana, 2014.

[21] I. I. Kim, B. McArthur, and E. J. Korevaar, "Comparison of laser beam propagation at 785 nm and 1550 nm in fog and haze for optical wireless communications," in *Proc. SPIE 4214*, *Optical Wireless Communications III*, Feb. 2001, pp. 26-37, DOI: 10.1117/12.417512.

[22] M. Ijaz, "Experimental characterisation and modelling of atmospheric fog and turbulence in FSO," Ph.D. dissertation, Faculty Eng. Env., Northumbria University, Newcastle upon Tyne, UK, 2013.

[23] M. Ijaz, Z. Ghassemlooy, J. Pesek, O. Fiser, H. Le Minh, and E. Bentley, "Modeling of fog and smoke attenuation in free space optical communications link under controlled laboratory conditions," *Journal of Lightwave Technology,* vol. 31, no. 11, pp. 1720-1726, June 2013, DOI: 10.1109/JLT.2013.2257683.

[24] M. S. Awan, L. Csurgai-Horváth, S. S. Muhammad, E. Leitgeb, F. Nadeem, and M. S. Khan, "Characterization of Fog and Snow Attenuations for Free-Space Optical Propagation," *Journal of Communications,* vol. 4, no. 8, pp. 533-545, Sept. 2009, DOI: 10.4304/jcm.4.8.533-545.

[25] International Telecommunication Union, "Calculation of free-space attenuation," Recommendation ITU-R P.525-4, Aug. 22, 2019. [Online] Available: https://www.itu.int/dms_pubrec/itu-r/rec/p/R-REC-P.525-4-201908-I!!PDF-E.pdf

[26] Z. Ghassemlooy, W. Popoola, and S. Rajbhandari, "Channel Modelling," in *Optical wireless communications: system and channel modelling with Matlab®*, 2nd ed. Boca Raton, FL, USA: CRC press, 2019, ch. 3, pp. 115-119.

[27] H. Henniger and O. Wilfert, "An Introduction to Free-space Optical Communications," *Radioengineering,* vol. 19, no. 2, pp. 203-212, June 2010. [Online] Available: https://www.radioeng.cz/fulltexts/2010/10_02_203_212.pdf

[28] W. O. Popoola, "Subcarrier intensity modulated free-space optical communication systems," Ph.D. dissertation, Faculty Eng. Env., Northumbria University, Newcastle upon Tyne, UK, 2009.

[29] A. Basahel, M. R. Islam, M. H. Habaebi, and S. Ahmad, "Availability prediction methods for terrestrial free-space-optical link under tropical climate," *Indonesian Journal of Electrical Engineering and Computer Science (IJEECS),* vol. 10, no. 1, pp. 224-229, April 2018, DOI: 10.11591/ijeecs.v10.i1.

[30] A. Prokes, "Atmospheric effects on availability of free space optics systems," *Optical Engineering,* vol. 48, no. 6, p. 066001, June 2009. DOI: 10.1117/1.3155431

[31] M. Handura, K. Ndjavera, C. Nyirenda, and T. Olwal, "Determining the feasibility of free space optical communication in Namibia," *Optics Communications,* vol. 366, pp. 425-430, May 2016, DOI: 10.1016/j.optcom.2015.12.057.

[32] A. Prokes and V. Skorpil, "Estimation of free space optics systems availability based on meteorological visibility," in *2009 IEEE Latin-American Conference on Communications*, 2009, pp. 1-4, DOI: 10.1109/LATINCOM.2009.5305266.

[33] O. O. Kolawole, T. J. Afullo, and M. Mosalaosi, "Initial Estimation of Scintillation Effect on Free Space Optical Links in South Africa," in *2019 IEEE AFRICON*, 2019, pp. 1-6, DOI: 10.1109/AFRICON46755.2019.9134032.

[34] D. A. Luong, T. C. Thang, and A. T. Pham, "Effect of avalanche photodiode and thermal noises on the performance of binary phase-shift keying-subcarrier-intensity modulation/free-space optical systems over turbulence channels," *IET Communications,* vol. 7, no. 8, pp. 738-744, May 2013, DOI: 10.1049/iet-com.2012.0600.

[35] M. Abaza, R. Mesleh, and A. Mansour, "Performance analysis of MISO multi-hop FSO links over log-normal channels with fog and beam divergence attenuations," *Optics Communications,* vol. 334, pp. 247-252, Jan. 2015, DOI: 10.1016/j.optcom.2014.08.050.

[36] A. Prokeš, "Modeling of atmospheric turbulence effect on terrestrial FSO link," *Radioengineering,* vol. 18, no. 1, pp. 42-47, April 2009. [Online] Available: https://www.radioeng.cz/fulltexts/2009/09_01_042_047.pdf

[37] L. C. Andrews, R. L. Phillips, and C. Y. Hopen, *Laser beam scintillation with applications*, vol. 99, SPIE press, Bellingham, Washington, USA, 2001.
[38] A. Prokes and L. Brancik, "Degradation of free space optical communication performance caused by atmospheric turbulence," in *2012 2nd International Conference on Advances in Computational Tools for Engineering Applications (ACTEA)*, 2012, pp. 338-341, DOI: 10.1109/ICTEA.2012.6462896.
[39] H. Akbar and Iskandar, "BER performance analysis of APD-based FSO system for optical inter-HAPS link," in *2015 1st International Conference on Wireless and Telematics (ICWT)*, 2015, pp. 1-5, DOI: 10.1109/ICWT.2015.7449232.
[40] M. I. Petković, G. T. Đorđević, and D. N. Milić, "BER performance of IM/DD FSO system with OOK using APD receiver," *Radioengineering,* vol. 23, no. 1, pp. 480-487, April 2014. [Online] Available: https://www.radioeng.cz/fulltexts/2014/14_01_0480_0487.pdf
[41] M. Bouhadda, F. M. Abbou, M. Serhani, F. Chaatit, and A. Boutoulout, "Analysis of dispersion effect on a NRZ-OOK terrestrial free-space optical transmission system," *Journal of the European Optical Society-Rapid Publications,* vol. 12, no. 18, pp. 1-6, Oct. 2016, DOI: 10.1186/s41476-016-0020-x.
[42] M. Abramowitz and I. A. Stegun, *Handbook of mathematical functions with formulas, graphs, and mathematical tables* vol. 55: US Government printing office, 1964.
[43] F. Scheid, *Schaum's outline of theory and problems of numerical analysis*: McGraw-Hill, 1988.
[44] A. K. Majumdar, "Free-space laser communication performance in the atmospheric channel," *Journal of Optical and Fiber Communications Reports,* vol. 2, pp. 345-396, 2005, DOI: 10.1007/s10297-005-0054-0.

Olabamidele O. Kolawole received his Bachelor of Technology degree in Physics (Electronics) from the Federal University of Technology, Akure, Nigeria in 2012 and a Master of Science degree in Electronic Engineering from the University of KwaZulu-Natal, Durban, South Africa in 2018. He is currently studying to obtain his Doctorate in Electronic Engineering at the University of KwaZulu-Natal, Durban, South Africa. He is a member of the IEEE Eta Kappa Nu (Mu Eta chapter) and a student member of the IEEE. His research interests include free space optics and RF propagation studies.

Thomas J.O. Afullo obtained his Bachelor's degree in Electrical and Electronic Engineering (Hons) from the University of Nairobi in 1979, MSEE from the University of West Virginia, USA in 1983 and the license in Technology and PhD in Electrical Engineering from Vrije Universiteit (VUB), Belgium in 1989. He is currently a Professor and Director for Centre for Radio Access and Rural Technology (CRART) in the School of Electrical, Electronic and Computer Engineering at the University of KwaZulu-Natal, Durban, South Africa. He is a member of the Eta Kappa Nu (MHKN), senior member, IEEE and a Fellow of the South African Institute of Electrical Engineers (FSAIEE). His research interests include RF and propagation studies in Africa, free space optics and power line communications.

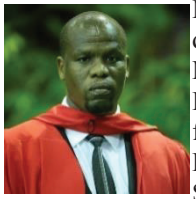

Modisa Mosalaosi received his Bachelor's degree in Electrical Engineering in 2009, MScEng and PhD degrees in Electronic Engineering in 2015 and 2017 respectively from the University of KwaZulu-Natal, Durban, South Africa. He is currently a Senior Lecturer at the Department of Electrical, Computer and Telecommunications Engineering, Botswana International University of Science and Technology, Palapye, Botswana. He is a member of the IEEE Eta Kappa Nu (Mu Eta chapter) and a professional member of the IEEE. His research interests include power line communications, RF and propagation studies and free space optics.

CONTENTS PAGE